23

OCT 20 1997

LIBRARY

EUROPEAN ORGANIZATION FOR NUCLEAR RESEARCH

CERN / SPSC 97–22
SPSC / P265 Add. 1
October 7, 1997

ADDENDUM to PROPOSAL SPSLC / P265

LOW MASS DIMUON PHYSICS IN NA50 UPGRADED BY ADDING A PIXEL VERTEX SPECTROMETER

M.C. Abreu[6,a], B. Alessandro[11], C. Alexa[2], R. Arnaldi[11], M. Atayan[13], C. Baglin[1], A. Baldisseri[10] A. Baldit[4], M. Bedjidian[12], F. Bellaiche[12], S. Beolè[11], V. Boldea[2], P. Bordalo[6,b], H. Borel[10], A. Bussière[1], M. Campbell[5,*], E. Cantatore[5,*], L. Casagrande[6], J. Castor[4], T. Chambon[4], B. Chaurand[9], I. Chevrot[4], E. Chesi[5,*], B. Cheynis[12], E. Chiavassa[11], C. Cicalò[3], M.P. Comets[8], S. Constantinescu[2], J. Cruz[6], V. Danielyan[13], A. De Falco[3], N. De Marco[11], G. Dellacasa[11,c], A. Devaux[4], S. Dita[2], O. Drapier[12], L. Ducroux[12], B. Espagnon[4], J. Fargeix[4], S.N. Filippov[7], P. Force[4], M. Gallio[11], Y.K. Gavrilov[7], C. Gerschel[8], P. Giubellino[11], M.B. Golubeva[7], M. Gonin[9], J. Gosset[10], A.A. Grigorian[13], J.Y. Grossiord[12], F.F. Guber[7], A. Guichard[12], H. Gulkanyan[13], R. Hakobyan[13], R. Haroutunian[12], E.H.M. Heijne[5,*], M. Idzik[11], D. Jouan[8], T.L. Karavitcheva[7], L. Kluberg[9] (Spokesman), A.B. Kurepin[7], Y. Le Bornec[8], C. Lourenço[5], P. Macciotta[3], M. Mac Cormick[8], A. Marzari-Chiesa[11], M. Masera[11], A. Masoni[3], S. Mehrabyan[13], A. Morsch[5], S. Mourgues[4], A. Musso[11], P. Petiau[9], A. Piccotti[11], J.R. Pizzi[12], G. Puddu[3], C. Quintans[6], L. Ramello[11,c], S. Ramos[6,b], P. Rato-Mendes[11], L. Riccati[11], A. Romana[9], I. Ropotar[5,d], S. Sartori[11], P. Saturnini[4], E. Scomparin[5,e], S. Serci[3], R. Shahoyan[6,f], S. Silva[6], M. Sitta[11], W. Snoeys[5,*], C. Soave[11], P. Sonderegger[5,b], F. Staley[10], X. Tarrago[8], P. Temnikov[3], Y. Terrien[10], N.S. Topilskaya[7], G.L. Usai[3], C. Vale[6], H. Vardanyan[13], E. Vercellin[11], N. Willis[8].

[1] LAPP, CNRS-IN2P3, Annecy-le-Vieux, France. LAPP
[2] IFA, Bucharest, Romania. Inst Phys.
[3] Università di Cagliari/INFN, Monserrato, Cagliari, Italy. U.
[4] LPC, Univ. de Clermont-Ferrand and CNRS-IN2P3, France. U.
[5] CERN, Geneva, Switzerland.
[6] LIP, Lisbon, Portugal. U.
[7] INR, Moscow, Russia. INR
[8] IPN, Univ. de Paris-Sud and CNRS-IN2P3, Orsay, France. IPN
[9] LPNHE, Ecole Polytechnique and CNRS-IN2P3, Palaiseau, France.
[10] CEA/DAPNIA/SPHN, Saclay, France†.
[11] Università di Torino/INFN, Torino, Italy. Turin U.
[12] IPN, Univ. Claude Bernard Lyon 1 and CNRS-IN2P3, Villeurbanne, France.
[13] YerPhI, Yerevan, Armenia. Yerevan Phys. Inst.
[a] Also at FCUL, Universidade de Lisboa, Lisbon, Portugal.
[b] Also at IST, Universidade Técnica de Lisboa, Lisbon, Portugal.
[c] Dipartimento di Scienze e Tecnologie Avanzate, II Facoltà di Scienze, Alessandria.
[d] Also at Bergische-Universität Gesamthochschule, Wuppertal, Germany.
[e] On leave of absence from Università di Torino/INFN, Torino, Italy.
[f] On leave of absence from YerPhI, Yerevan, Armenia.

*Consulting on the technical aspects of the Pixel detectors.
†Pending approval by DAPNIA authorities.

CERN-SPSC-97-22

Fermilab Library
0 1160 0076910 3

Contents

1 Introduction and Summary **1**

2 Detector Layout **3**

3 Track Simulation, Pattern Recognition, Track Matching **6**

3.1 Introduction 6

3.2 The event generator 7

3.3 Track recognition and matching 7

3.4 Results in the Vector Meson Region 12

3.5 $D\bar{D}$ decays 13

3.6 p-A runs 13

3.7 Background not related to the struck nucleus 14

4 New Physics Becomes Potentially Accessible **14**

4.1 Excess: more events observed in B-A than expected from p-A 14

4.2 Hadrons in dense and hot medium 14

4.3 Other mechanisms may produce excesses 15

4.4 Can experiment discriminate among mechanisms? 15

5 Detector Lifetime Under Irradiation **16**

6 Data Rate and Achievable Luminosities **17**

7 Test and Data Taking Program, Beam Time Requests **19**

7.1 First tests 19

7.2 Present and future plans 20

7.3 p-A programme 22

7.4 Beam time requests 22

8 Responsibilities and Budget **22**

1 Introduction and Summary

The Dilepton channel is characterized by its very *low production cross section*, and by the relevance of both *hard* (J/ψ, ψ', Drell-Yan pairs, $D\bar{D}$ decays) and *soft contributing processes* (thermal dileptons, ρ, ω, ϕ). Like most dimuon experiments, NA38/50 relies on a $\sim$ 5 m long wall, which absorbs the unscattered beam as well as all produced particles except muons, provided they are energetic enough to traverse the wall ($p_z \gtrsim 4$ GeV/c). While the particle flux produced in the target can be very high, the downstream spectrometer is hadron-free and defines a wide acceptance dimuon trigger. NA50 explores cross sections lower by several orders of magnitude than other experiments of comparable data acquisition capacity.

A price had to be paid so far: while the momenta of the muons can be quite accurately measured, their angles are blurred by multiple scattering in the absorber, which limits the resulting mass resolution to $\sigma_M \simeq 80$ MeV/c^2. The Pixel detectors developed by RD19 and used by the WA97 experiment, have now reached the resolution in space (pixel size 50·500 μm^2) and time (strobe width 30 - 200 ns) needed to overcome this limitation. The 3-momenta of the muons are measured, together with hundreds of hadrons produced in the same reaction, before they enter the absorber. The muons are recognised thanks to a *comparison of angles and momenta measured* in the spectrometers *before and after the absorber.*

A dedicated Low Mass ('ϕ') Setup (light absorber, reduced magnetic field, single short target), for studying ρ/ω and ϕ production, called hereafter NA50-Now, is part of the accepted NA50 Proposal (CERN-SPSLC 91-55). *We propose to upgrade the Low Mass Setup* by implanting *a vertex spectrometer* in the 25 cm long interval between target and hadron absorber, *equipped with Pixel detectors* in a 2 T dipole field. This setup, called in short NA50-Up, is described in Section 2. As shown in Section 3, which deals with the *event simulation*, it improves the muon angular resolution tenfold, and reduces the decay background (indeed, the π and K decay muons seldom satisfy the matching criteria). *New physics* (see Section 4) becomes accessible:

i) The mass resolution is $\sigma_M/M_{\mu^+\mu^-} \simeq 2.5\,\%$ and allows to *measure ρ and ω production separately*, for the first time in heavy ion physics. Thanks to the fact that leptons which originate inside a Hadron Gas (HG) will leave it undisturbed, and to the very short lifetime of the ρ meson ($\tau_\rho = 1.3$ fm/c), the *lifetime of the HG* can be estimated from the increased $\rho \to l^+l^-$ decay rate relative to $\omega \to l^+l^-$ ('fast ρ clock') [1] (the lifetime of ω and ϕ mesons is much larger, so they are hardly affected by a *HG* whose lifetime is $\tau_{HG} < 10$ fm/c, as found by pion interferometry). On the other hand, the *masses and widths* of particles in a hot HG may well *differ from those in vacuum.* The ρ signal may then be wider and shifted away from the nominal mass (ρ mass shift) [‡]. This phenomenon is one of the two most *fundamental research goals* in dilepton experiments in heavy ion collisions. But it also makes the ρ decays inside the HG a lot less easy to recognize, and the 'fast ρ clock' less straightforward. A Technical Note [2] reviews the theoretical status of the fate of vector mesons in a hot and baryon rich medium.

ii) The muon tracks are extrapolated to the target with an accuracy of 50 μm in each transverse direction, sufficient to *separate the $D\bar{D}$ decay pairs from the prompt muon pairs.* The *$D\bar{D}$ production cross section* can thus be directly measured, hence completing the charmonium systematics. Also, this will serve to prepare dilepton physics at LHC energies, where open charm and beauty will be used to monitor charmonium and bottomium suppression, the Drell-Yan signal being dwarfed by muon decays of charm and bottom mesons.

[‡]Several among us are indebted to I. Tserruya for having introduced us to the beauty and feasibility of rho mass shift studies.

All heavy ion dilepton experiments at the SPS have found *excesses* over expectation based on p-A results, in the mass regions below ($M_{l^+l^-} \approx 0.5$ GeV/c^2) and/or above the low mass resonances ($M_{l^+l^-} \approx 1.5$ GeV/c^2) [3]. The agreement is less impressive at the quantitative level. Phenomenological analyses have mostly dealt with the *low mass* e^+e^- *excesses* found by CERES and others, and related them to the ρ *mass shift* and broadening [2]. In Section 4, we emphasize that there are several mechanisms which may cause an 'excess' in the above sense, and few experimental clues to discriminate between them (the p_T dependence, probably [§], and perhaps the $\rho - \omega$ interference pattern).

We look forward to a new vitality of this physics thanks to the joint effort of CERES and NA50. The two upgraded experiments will study the same processes with vastly different acceptance windows and backgrounds. While NA50-Up cannot compete with the anticipated CERES mass resolution, we expect to reach better statistics, especially at high p_T.

NA50-Up will also measure the ϕ/ω ratio, with less systematic errors than the earlier *strangeness enhancement* studies based on the $\phi/(\rho + \omega)$ ratio [4]. It will become possible to control the procedures used to subtract the π, K decay background (overwhelming in NA50-Now).

The achievable luminosity is presently limited by the radiation tolerance of the Pixel detectors, discussed in Section 5. The 'OMEGA3/LHC1' chip (called hereafter LHC1), in production since end 1996, was found to sag after a radiation dose of 20 krad, while its predecessor, 'OMEGA2', survived 40 krad. A first prototype of the forthcoming 'LHC2/ALICE1' chip (called hereafter LHC2) was delivered this summer. An exposure to 800 krad from an X ray source resulted in no damage. This remarkable result allows to envisage very high interaction rates. The pixel size should be smaller (maybe 50·300 μm^2, as foreseen for ALICE), which would improve the track matching performance. To fully exploit the LHC2 potential, the readout should be faster than the present VME system; also, while not strictly compulsory, good timing (strobe < 100 ns, like in LHC1), would be desirable (see Section 6).

Let us note here that even the LHC2 Pixel spectrometer would not stand the extreme radiation load of the 1996 Pb-Pb $\rightarrow J/\psi$ run [5] ($\sim$ 1 Mrad/week), whose spectacular results were based on dimuon masses $M_{\mu^+\mu^-} > 3$ GeV/c^2. In fact, in this mass region the vertex spectrometer would bring little gain in mass resolution or background reduction.

The two main physics scopes correspond to different *running conditions* (Section 6):

i) For studying the possibly mass shifted ρ, and understanding the low mass excess, good acceptance down to low p_T is needed. This can be obtained, at the expense of decreasing luminosity (increased trigger rate), by changing the muon spectrometer parameters. The LHC1 chip is adequate under these conditions.

ii) Good statistics are compulsory for measuring $D\bar{D}$ decays and for understanding the intermediate mass excess ($M_{\mu^+\mu^-} \sim 1.5$ GeV/c^2). The needed high luminosity configuration is well served by a vertex spectrometer based on LHC2 chips with good timing and fast readout.

Section 7 describes the results obtained in beam tests done in last November and April. We then stress the need of reliable p-A reference data, obtained in the same apparatus. Beam requests for p and Pb runs in 1997 and 1998, and suggestions for 1999/2000, serve the following goals:

i) a *verification of the achievable mass resolution* in p-A reactions in winter 1997/98;

ii) a measurement of the ρ/ω *ratio and interference pattern* in p-A;

[§] J. Schukraft has drawn our attention to this crucial point, which has been little discussed in the literature.

iii) a Pb *beam run* on *Vector Meson physics* in 1998; and

iv) with a LHC2 detector, *high luminosity runs* with p and Pb beams for *open charm* and *high* p_T systematics.

Finally, Section 8 describes the budget and responsibilities.

2 Detector Layout

Pixel detectors are made of finely segmented Si detectors and equally segmented miniaturized readout and control electronics (typically 10^6 transistors per cm^2). Each detector segment ('pixel') is individually bonded to the corresponding electronics cell [6] (see Fig. 1). Their total thickness is presently 1 mm, i.e. $2 \cdot 300$ μm Si (detector plus electronics) plus a 400 μm thick ceramic support, which vehiculates the information.

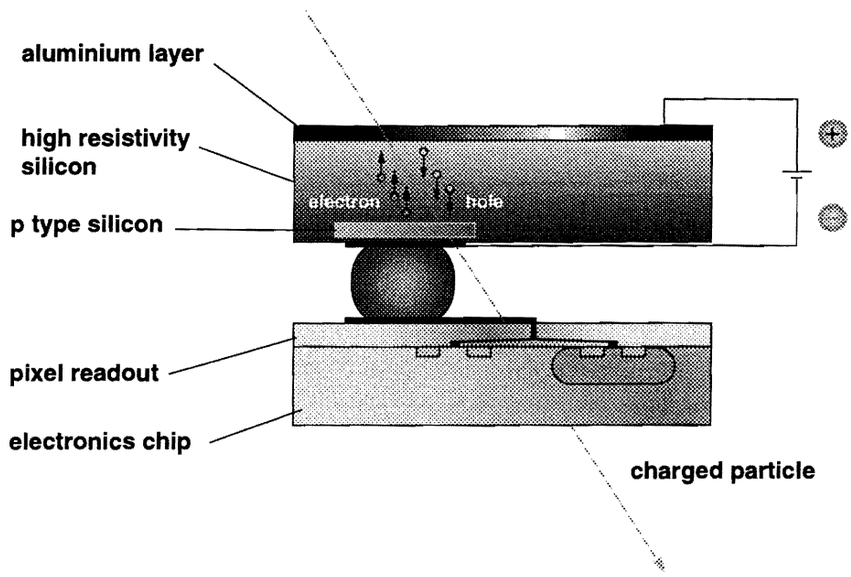

Fig. 1.: The basic LHC1 pixel element: detector (*top*), bonded by a tiny 20 μm Sn ball to the electronics element (preamplifier, discriminator, tunable delay, validation by trigger signal, memorization in shift register); both $50 \cdot 500$ μm^2 area, $2 \cdot 300$ μm thickness. A chip contains 2048 pixel channels.

These detectors have been pioneered by the CERN Microelectronics group, and developed by the RD19 and WA97 Collaborations in view of their use in experiments WA97 and NA57. The basic building block is the LHC1 chip, made of 2048 pixels of size $50 \cdot 500$ μm^2. Units of 6 chips, so called *ladders*, have been mass produced. Ladders are mounted on a ceramic support to form an *array*, which is connected to a readout board. Two staggered arrays form a half plane (top or bottom).

The LHC1 chip will be replaced in due course by the more radiation tolerant LHC2 chip (see Section 5).

The proposed NA50-Up layout detects the charged particles emitted into the NA50 acceptance ($35 < \theta_\mu < 110$ mrad). Fig. 2 shows *two layout versions.* We have started building a minimal layout of 4 planes of LHC1 detectors ($\sim$ 130 000 channels, see top of Fig. 2), which

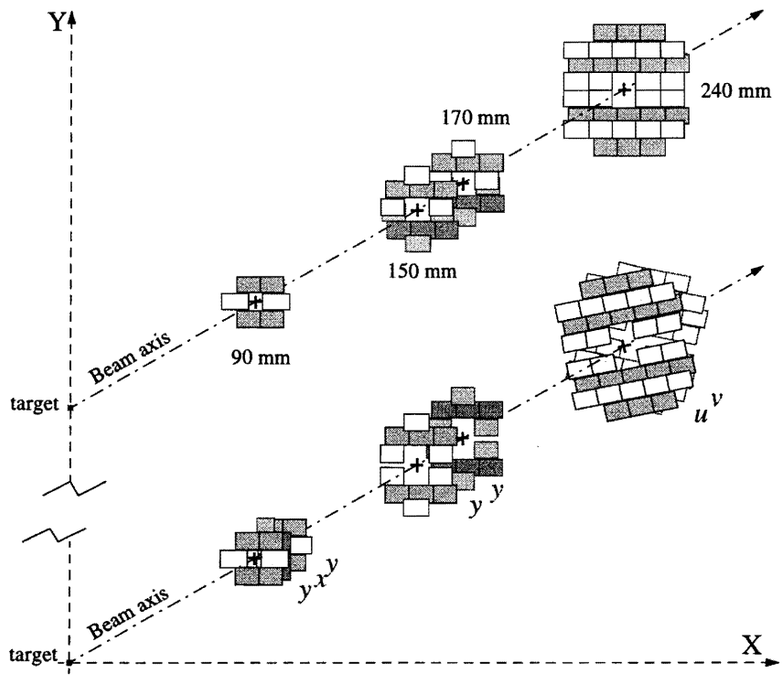

Fig. 2.: Two versions of the *detector layout* are sketched: one of 64 LHC1 chips (Top) for studying low mass resonances, and a more ambitious one (Bottom), based on the forthcoming LHC2 chip, and capable of extrapolating the muons to the target plane with sufficient accuracy to *distinguish* D *decay muons from prompt muons.* Distances from the target are indicated. All top planes, as well as the bottom ones labelled y have the pixels oriented horizontally, along the magnetic field, in order to measure well the curvature in the Y-Z plane. Accurate tracking in the X-Z plane is provided, in the bottom layout, by an x detector plane whose chips are turned by 90°, and a u and a v plane inclined to the horizontal by ±180 mrad.

should be adequate for a first look at the physics of the ρ, ω and ϕ vector mesons. While most of the detector structures are made of 6-chip ladders, only the actually used chips are shown.

A more evolved layout based on the forthcoming LHC2 chip might look like the lower sketch of Fig. 2. It uses *3 stations* consisting of 2 or 3 planes each, to ensure a proper coverage of the solid angle (90 % of all NA50 trigger muons are seen in at least 3 planes), eased pattern recognition (for most tracks, the station gives not only the position, but also a local direction), a degree of redundancy (a track is well measured even if 1 or 2 hits are missing), and good accuracy in both transverse planes, so that $D\bar{D}$ decay pairs can be recognized.

A small magnet (the revamped TC8 magnet of overall length 55 cm, 8 cm gap, 2 T field), called hereafter 'pixel magnet', houses the single 1 mm thick Pb target, the halo counter used to control the beam position and width, and the detector planes, located between 9 and 24 cm downstream of the target (see Fig. 3). The first, 60 cm long Al_2O_3 section of the hadron absorber starts at 26 cm, still inside the magnet. The overall structure of the vertex spectrometer can be seen in Fig. 4.

Figure 5 shows the impacts of the muons which trigger the NA50 spectrometer, at 24 cm

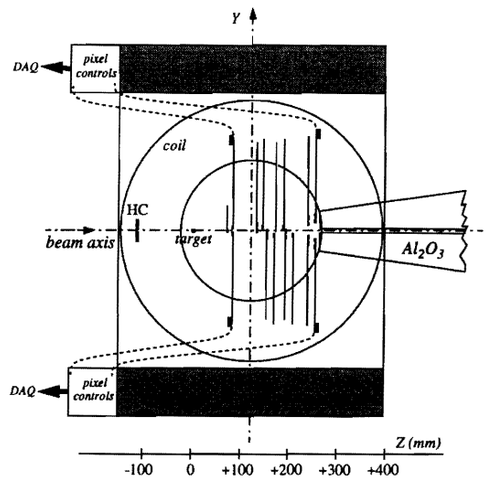

Fig. 3.: The vertex region. The TC8 magnet houses the Halo Counter (HC), the Pb target, the Pixel detectors, and the beginning of the hadron absorber. Not shown: the retracting mechanism used to remove the Pixel detectors during beam tuning or instability.

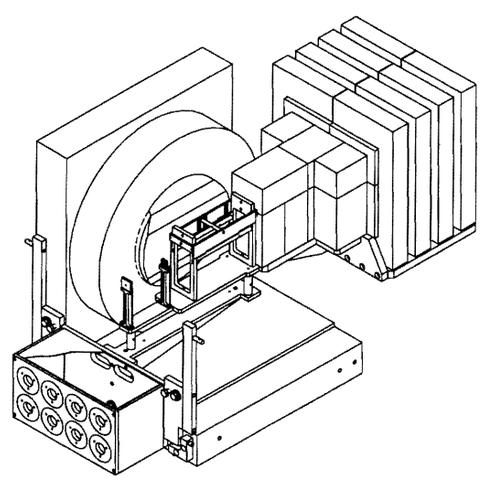

Fig. 4.: Drawing of the support structures. Along the beam, from left to right: halo counter, target, top half of the detectors, and first absorber section; roof and front yoke of the magnet are not shown.

from the target, and their coverage by the Pixel plane located there. The sextant structure of the muon spectrometer is clearly seen. The magnetic field is parallel to the (horizontal) X axis, with charged tracks deflected in the Y-Z plane. The Pixel planes are split in top and bottom halves.

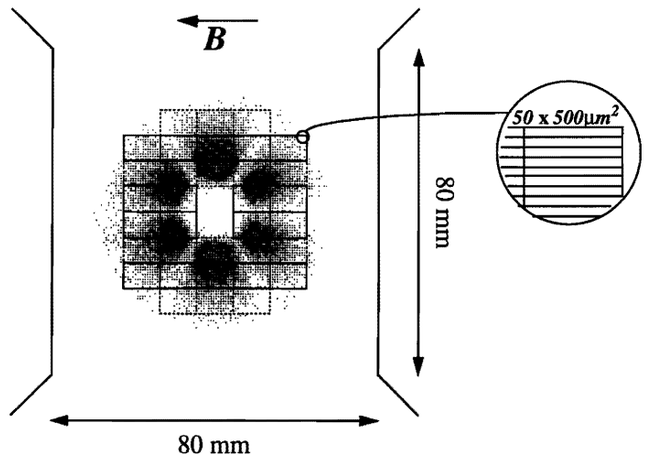

Fig. 5.: Impacts of trigger muons at station 3 (24 cm from the target), and active areas of the corresponding Pixel chips, which are mounted on a front and a back *arrays* (solid and dashed rectangles). The pixels are oriented parallel to the magnetic field **B**; the limits of the shimmed magnet poles are shown.

Most pixels are oriented parallel to the magnetic field, to measure accurately the track deflection in the Y coordinate ($'y'$-planes). A resolution in X sufficient to ensure *extrapolation to the vertex (target)* with a precision of $\sigma_{v,X} \simeq \sigma_{v,Y} \approx 50$ μm, needed to identify the $D\bar{D}$ events, is obtained by inserting an $'x'$-plane between the 2 $'y'$-planes closest to the target, and by tilting the last two planes by ± 180 mrad.

The detectors can be retracted when the beam is being aligned. When the beam becomes unstable, a Pixel Safety System takes over: the halo counter sends a signal to stop one beam magnet, and no further beam can reach NA50 until that magnet has been restored.

Finally, a cooling system blows cold air into the magnet, to prevent the detectors from overheating.

3 Track Simulation, Pattern Recognition, Track Matching

3.1 Introduction

A configuration of 4 pixel planes at 8, 15, 17 and 24 cm has been extensively simulated under the conditions given for the topmost case of Fig. 14. The 3 stations, 7 planes configuration gives similar resolution, better efficiency and some redundancy. Indeed, a separate study has shown that adding extra material does not affect the mass resolution, the muon momenta being determined mainly by the muon spectrometer's magnet (the ACM magnet).

3.2 The event generator

An *event generator* has been developed, which reproduces the observed $\mu^+\mu^-$, $\mu^+\mu^+$ and $\mu^-\mu^-$ spectra, as well as the experimentally measured trigger rates. The soft particle production follows a thermal model, while the hard processes (Drell-Yan and open charm production) are generated by Pythia 5.7.

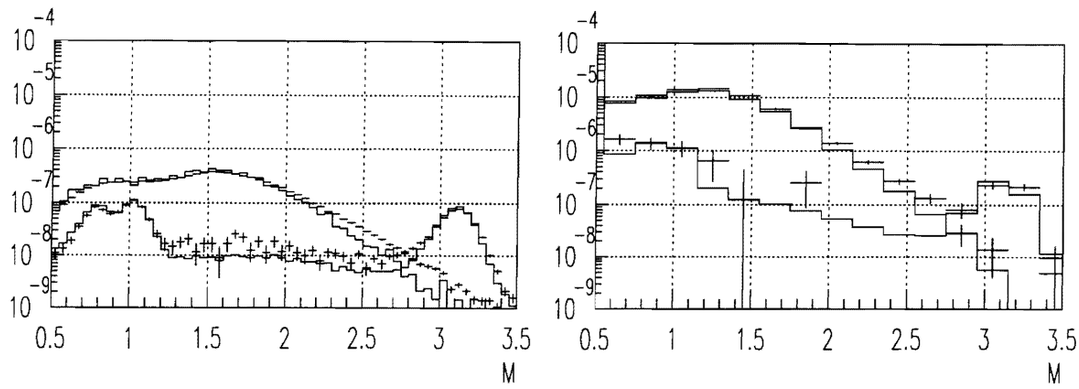

Fig. 6.: Experimental (points with error bars) and generated (solid line) mass spectra, normalized per one average interaction. Signal and Background are shown separately: the former shows the characteristic resonances peaks. The Left plot is obtained with 7 kA in the ACM magnet (1995 Pb-Pb data), the Right plot with 4 kA (2 runs from 1995 Pb-Pb data).

The produced charged particles are tracked through the Pixel spectrometer, allowing for multiple scattering in the target and in the detectors (each plane corresponds to 1.9 % X_0).

Vector mesons, π's and K's are forced to decay to muons, which are then weighted correspondingly. The DIMUJET simulation program tracks the muons through the NA50 setup.

In Fig. 6 two experimentally measured dimuon mass spectra are compared with generated spectra which were computed for the same NA50-Now absorber and field configurations, and normalized to the same number of interactions. The spectra for signal and background are considered separately. The Left plot is obtained with a current in the muon spectrometer of 7 kA, while the Right one is for 4 kA. The generator results are in good agreement with the data except for the discrepancies at high masses, in the case of the background spectrum, which can be ascribed to the too soft high p_T tail of the Boltzmann distribution.

3.3 Track recognition and matching

The *track recognition and matching* procedure for *prompt muons* follows several steps.

- The *pattern recognition* of the tracks is done by fitting the hits in the various Pixel planes. Presently we are fitting the tracks by line and parabola in X and Y directions respectively. We are considering the possibility of using the tabulated trajectories method [8].
- The *interaction vertex determination.* The extrapolation of the tracks to the vertex allows to measure the transverse coordinates in the vertex plane with an accuracy of σ_{xyv} = 55 μm. Thus the common *interaction vertex* can be determined to high precision (less

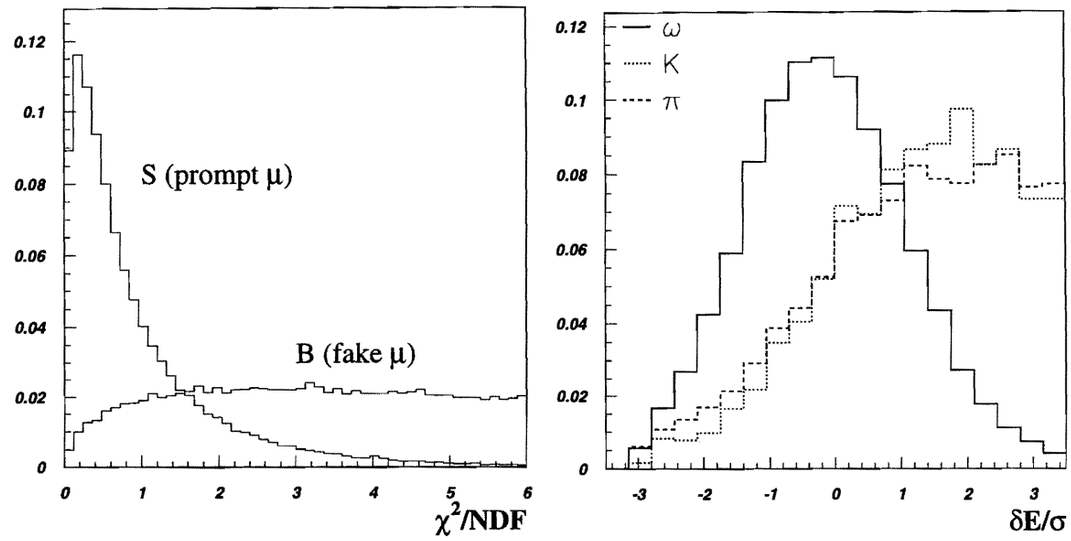

Fig. 7.: Left: Distributions of χ^2 per degree of freedom, for genuine μ's and fake matches, normalized to unity. Right: Normalized distribution of $\delta E/\sigma$ (see text) for prompt ('ω') and decay muons. For most of the matched decay muons, the Pixel spectrometer measures the energy of the parent meson, hence the $\delta E/\sigma$ is shifted towards the positive values.

than 10 μm) for a few tens of tracks already. The vertex is used as an additional constraint to fit the candidate tracks (except when $D\bar{D}$ pairs are studied).

- Among all the tracks recognized in the Pixel spectrometer, the *candidates* to match the muon reconstructed in the muon spectrometer, $\mu^{(\text{real})}$, are found by building the weighted square of differences (hereafter called *matching* χ^2) of their *inverse momenta, azimuthal* and *polar angles* with those of $\mu^{(\text{real})}$. The error matrix used has been determined from simulated events.

  These candidate tracks correspond both to real muons and to wrongly matched tracks or *fakes*, which are mainly hadrons which have a better χ^2 than the real muon. In order to make a distinction between these two contributions, for each sample with a given χ^2, we use the probability of having i candidates is defined as :

$$P_i(\chi^2) = (1 - P_o)S(\chi^2) + (P_o + i - 1)B(\chi^2)$$

  where $S(\chi^2)$ and $B(\chi^2)$ are the two probabilities of having respectively genuine μ's and fake matches for this χ^2, and P_o is the probability that the real muon track is missing in the set of the candidates. This last quantity is the only one which is extracted from the Monte-Carlo simulation. $S(\chi^2)$ and $B(\chi^2)$ can be obtained by comparing samples with i and j candidates. What is precisely done is to calculate the average over all possible (i,j) combinations according to their respective errors. The resulting $S(\chi^2)$ and $B(\chi^2)$ distributions are shown in Fig. 7 When the real muon is matched, the distribution peaks near zero while it is wide for wrong matches.

- After rejection of the tracks with bad matching χ^2, the surviving tracks are fitted again, this time using the curvature measured for the corresponding μ in the muon spectrometer. In fact, the total momentum resolution of the muon spectrometer is always better than the resolution of the Pixel spectrometer.

- A further rejection of the background and of the fakes can be achieved applying a cut on the variable:

$$\frac{\delta E}{\sigma} = \frac{E_{PIX} - E_{NA50}}{\sqrt{\sigma(E_{PIX})^2 + \sigma(E_{NA50})^2}}$$

  where E_{PIX} and E_{NA50} are the muon energies measured in the Pixel and NA50 spectrometers respectively. Fig. 7-Right shows the δE distribution for the muons generated by ω, π and K decays.

  The distribution is asymmetric for the fakes, since most charged hadrons which might match the real muon have a lower energy than the muon itself. For the background tracks, the Pixel detector measures mainly the π or K which later decays to a μ with smaller energy, measured in the muon spectrometer.

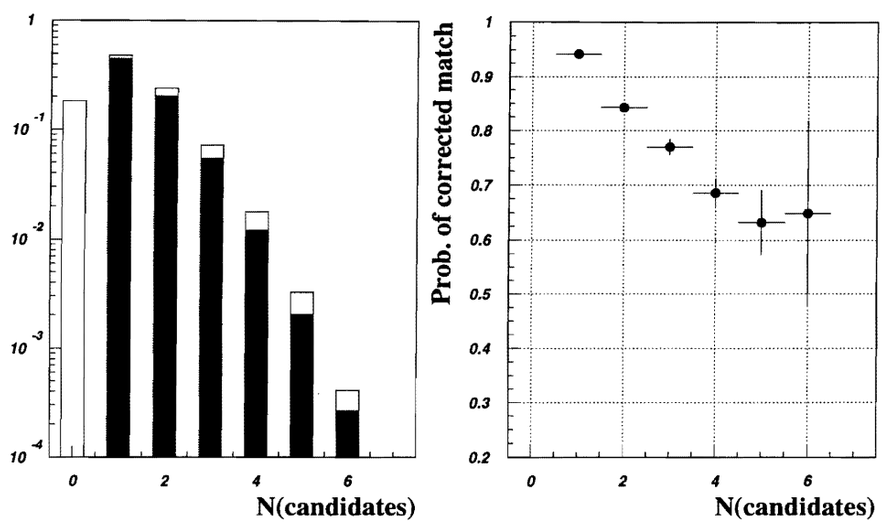

Fig. 8.: Left: Distribution of the number of candidate tracks, i.e. those passing the cut on the matching χ^2 (hollow bars). The distribution of true matches, for which the muon track has the smallest matching χ^2, is superimposed as solid bars. Right: Probability of selecting the correct muon track versus the number of candidates.

- The *final decision* to associate the track with the smallest χ^2 to the muon depends on the number of candidates found. The average number of candidates is roughly proportional to dN_{ch}/dy. Fig. 8 shows the distribution of the number of candidate tracks for $dN_{ch}/dy = 180$, corresponding roughly to the average charged multiplicity of the Pb-Pb collisions selected by the NA50 dimuon trigger.

  If n candidates are found, the probability that the candidate with minimal $\chi^2 = \chi_1^2$ corresponds to the real muon is:

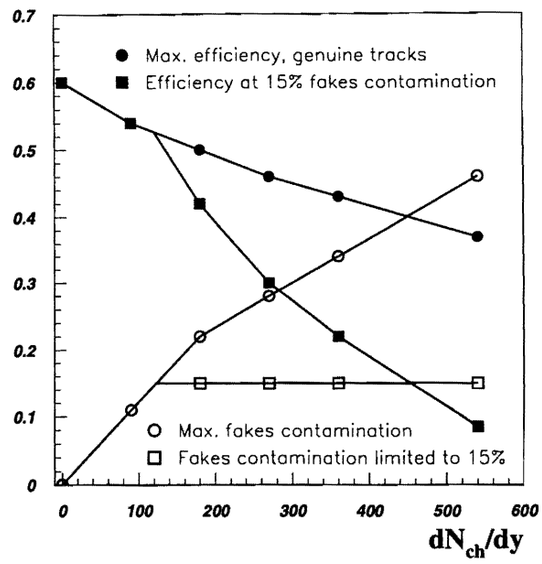

Fig. 9.: Genuine dimuon matching efficiency, fraction of fakes, and efficiency corresponding to 15 % fake contamination, versus dN_{ch}/dy. p-A runs correspond to $dN_{ch}/dy < 10$, central Pb-Pb events to $dN_{ch}/dy \simeq 360$.

$$P_1(\chi) = \frac{(1-P_o)S(\chi_1^2) \times \prod_{i=2}^{n} B(\chi_i^2)}{P_o \prod_{i=1}^{n} B(\chi_i^2) + (1-P_o) \sum_{i=1}^{n} S(\chi_i^2) \prod_{j \neq i}^{n} B(\chi_j^2)}$$

where $S(x)$ and $B(x)$ are the two χ^2 distributions of Fig. 7 and P_o is the probability that the real muon track is missing in the set of the candidates. The probability that both the tracks of a dimuon event are correctly matched is simply $P_{dimuon} = P_1(\chi^2_{min1}) * P_2(\chi^2_{min2})$. Thus, setting a threshold, P_{cut}, on this parameter, we can decrease the fraction of fake tracks to the wanted level (while losing some matching efficiency).

Fig. 9 shows the matching efficiencies and fake contamination as a function of the charged multiplicity per unit of rapidity. For the chosen detector layout $\sim$ 5% of the muons are missed in each of the 4 planes, so the dimuon acceptance, and hence the ideal matching efficiency, is 65 %.

The resulting (mis)matching efficiencies for signal and background dimuons are plotted versus the P_{cut} value in Fig. 10 (Middle) plots for $dN_{ch}/dy = 180$ and 360. One may check that the 15 % fake dimuon contamination of Fig. 9 is obtained for $P_{cut} = 0.63$ and 0.80, respectively.

The Top plots of Fig. 10 show the mass resolution, both before ('genuine + fake') and after ('genuine') elimination of the mismatched tracks. Here, we compute the standard deviation σ by the 'Polish method', as half of the interval containing 2/3 of the events. The Bottom plots show the fake dimuon contamination. It should be noted that mismatched dimuons usually contain one correctly matched μ.

Since the π and K decay muons are rarely matched, the majority of selected background dimuons are mismatches. With P_{cut} chosen to limit the fakes to 15 % of the genuine dimuons,

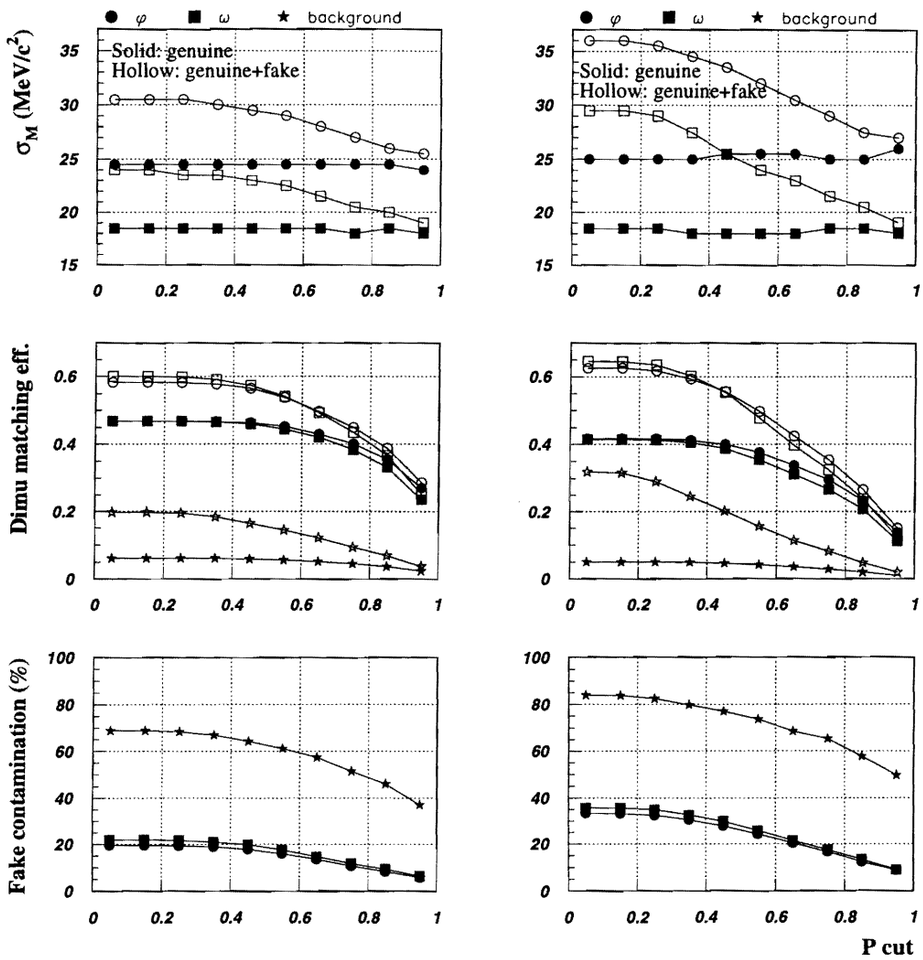

Fig. 10.: Dimuon mass resolution, matching efficiency and contamination by fake matches for (Left) $dN_{ch}/dy = 180$ and (Right) $dN_{ch}/dy = 360$.

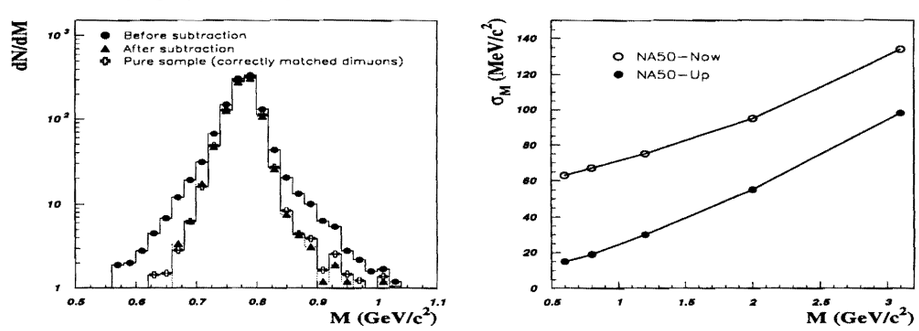

Fig. 11.: Left: Mass spectrum for matched ω's with 20% fake contamination, and after subtraction of the fakes (mixed event technique). For comparison the true spectrum of correctly matched pairs is also shown. Right: Dependence of the mass resolution on the dimuon mass for correctly matched tracks.

the Background/Signal ratio after track matching is 4 times smaller than for the original NA50 dimuon trigger sample.

The remaining fake events can be subtracted using the *mixed events technique*: we can generate a 'pure fakes sample' by associating a trigger μ with candidate Pixel tracks from events with no μ in the corresponding sextant. Fig. 11 (Left) shows the result of such fakes subtraction for simulated ω events ($dN_{ch}/dy = 180$).

Fig. 11 (Right) shows the mass resolution for the correctly matched dimuons (as it would be after the fakes subtraction) as a function of dimuon mass. The pairs in which one of the matched muons is a fake have mass resolution similar to what we have in NA50-Now.

3.4 Results in the Vector Meson Region

The resulting mass spectra and signal to background ratios for the proposed NA50-Up setup are shown on Fig. 12, where they are also compared to NA50-Now. In both setups the current in the muon spectrometer's magnet is 3 kA and the last 20 cm of C absorber are replaced by iron. In the case of NA50-Up the beginning of the absorber is at 25 cm from the target to leave room for the Pixel detectors, while it is at 10 cm in NA50-Now.

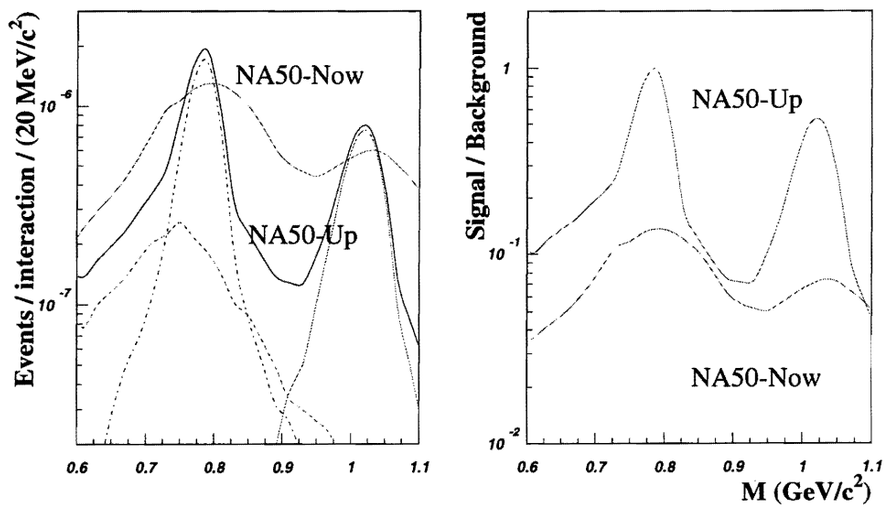

Fig. 12.: Normalized *mass spectra* (Left) and *signal to background ratio* (Right) for NA50-Now and NA50-Up. Resonances ρ, ω and ϕ are shown for NA50-Up (dotted curves). Continuum is included but not shown explicitly.

The vector meson spectra are indicated separately and without interference term for ρ, ω and ϕ. The 15 % fakes are not subtracted. A realistic run of 10^{10} interactions produces several thousand of ρ's in the regions where its tail dominates over the other contributions.

For a realistic analysis, good p-A reference data will be needed, in particular to establish the basic $\rho - \omega$ interference pattern in conditions of low background.

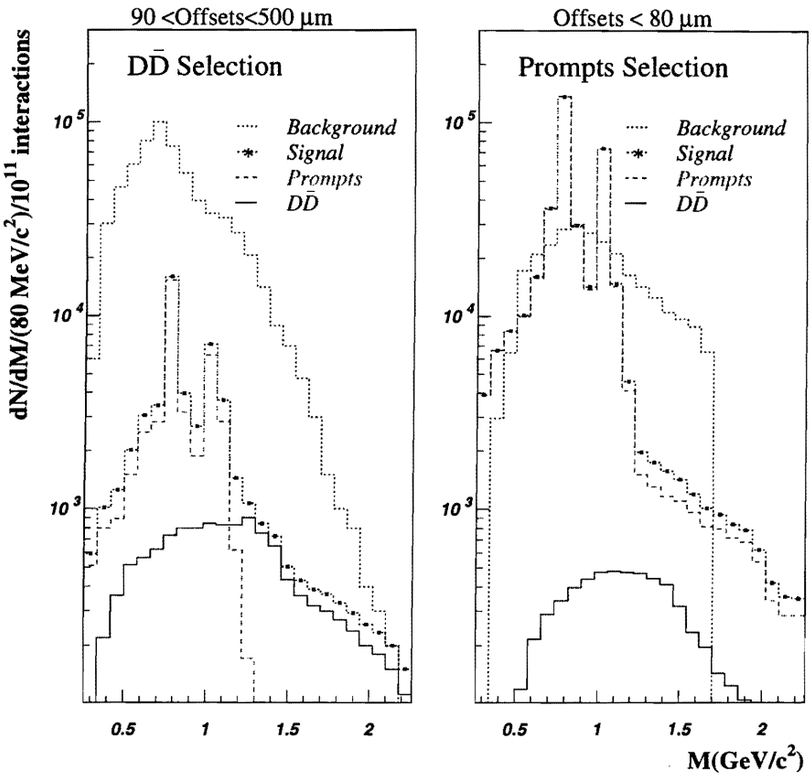

Fig. 13.: The dimuon mass spectra can be strongly enriched in $D\bar{D}$ decays (Left, intermediate minimal distances of the extrapolated muon tracks from the interaction vertex), or in *prompt muon pairs* (Right, tracks compatible with origin in the interaction vertex).

3.5 $D\bar{D}$ decays

For the analysis of muon pairs from $D\bar{D}$ decays, the procedure differs only by a looser vertex constraint and by an additional cut on small measured offsets at the interaction plane.

As it was mentioned, the good offset resolution allows to analyse the data in two modes: in view of $D\bar{D}$ *enrichment*, selecting only tracks with offsets on the range typical for D decays (few 100 μm, thus rejecting most prompt and some π and K decay muons; and of *prompt dimuon* (small offset) *selection*, suppressing both from $D\bar{D}$ and many π and K decays. Fig. 13 shows the contributions to the mass spectra for these two modes. The selection of intermediate offsets produces an almost pure $D\bar{D}$ signal (after background subtraction) for $M_{\mu+\mu-} \geq 1.2$ GeV/c^2. Indeed, the $D\bar{D}$ to *prompt* ratio jumps from $\sim 1/4$ for $M_{\mu+\mu-} < 1.2$ GeV/c^2 (except for the ω and ϕ peaks) to 4/1 between 1.2 and 2 GeV/c^2.

3.6 p-A runs

To first order, 200 p-Pb collisions produce the same secondaries as one central Pb-Pb collision. However, only those which happen within 20 ns, the time resolution of the dimuon trigger, can cause a random $\mu^+\mu^-$ trigger, usually with both muons due to meson decays. Therefore, the

Background/Signal ratio is always small (at 10^9 protons per 2 s burst on a 1 mm Pb target, the background is only 12 % higher than at low intensity running). Furthermore, the Pixel spectrometer only accepts pile-up hits during its trigger strobe width, which is $\lesssim$ 40 ns for station 1, and $\lesssim$ 200 ns for the detector arrays which feature more than 2 LHC1 chips. In the above example, the $dN/dy \simeq 5$ intrinsic p-Pb multiplicity will therefore be roughly doubled, the occupancy and the background-to-signal ratio being still very small.

3.7 Background not related to the struck nucleus

Two potentially dangerous background sources have been studied and simulated. Most of the δ-rays produced in the target and elsewhere, which constitute a non negligible background in the *Multiplicity Detector* of the present NA50 configuration, are swept away by the pixel magnet and do not reach the detectors.

Concerning the secondaries which produce showers inside the magnet shims, a GEANT simulation has shown that these increase the particle density on the last plane by only 4 %.

4 New Physics Becomes Potentially Accessible

In this Section, we deal mainly with the experimentally observed (low mass) 'excess', the theoretical activity on medium induced modifications of vector meson spectra [2], and the problems faced by the experimentalist trying to relate measured data to underlying reaction mechanisms.

4.1 Excess: more events observed in B-A than expected from p-A

HELIOS-3, NA38 and CERES find excess events over the extrapolation from p-A data [3] for ^{32}S reactions with heavy targets, and CERES also for ^{208}Pb beams, in two regions outside the resonances: Low ($M \lesssim 0.6$ GeV/c^2) and Intermediate mass continuum ($1.2 \lesssim M \lesssim 2$ GeV/c^2). The two customary normalizations — dimuons/Drell-Yan pairs for NA38/50, dileptons/charged particles for the HELIOS-3 and CERES experiments — are inspired from different physics: hard (cross sections $\propto$ A $\cdot$ B) and soft (same temperature, same A, B dependence for all hadrons). The resulting relative normalization coefficients which relate B-A to p-A dilepton spectra are found to be almost identical. However, the excesses observed by these three experiments appear to be quite different in magnitude, and a consistent evaluation of these data, at the quantitative level, is not yet available.

4.2 Hadrons in dense and hot medium

In a Hadron Gas (HG), hadrons live in thermal and, to some extent, chemical equilibrium with each other.

The size and lifetime of the HG are studied, by WA98, NA44 and NA49, via Hanbury-Brown–Twiss (HBT) Interferometry [9]. While the transverse radius is found to be $R \simeq 6$ fm for Pb-Pb collisions, the lifetime is more tricky, but certainly not large, contrary to early expectations; the upper limits for τ_{HG} vary between 1 fm/c and 13 fm/c.

We treat first the case where the changes of masses and widths can be neglected. The interesting case is the ρ meson, whose lifetime ($\tau_\rho = 1.3$ fm/c) is shorter than the indicative

hadron gas lifetime. Several generations of ρ's will succeed each other and have a chance to decay to dileptons. The apparent $\rho \to l^+l^-$ decay rate, as monitored by the $\omega \to l^+l^-$ decay will increase in a HG as

$$\frac{\rho \to l^+l^-}{\omega \to l^+l^-}|_{HG} \simeq \frac{\rho \to l^+l^-}{\omega \to l^+l^-}|_{p-p} \cdot (1 + \tau_{HG}/\tau_\rho \cdot f(p_T))$$

This is the so called 'fast ρ clock'. The $f(p_T)$ term indicates the possibility that the excess term may be characterized by a measurable *difference in p_T dependence* (a ρ of high p_T may leave the HG before decaying).

Recent studies have led to the expectation that hadrons may have their masses, widths and other properties altered by the medium, just like nucleons in nuclei or electrons in solid state physics. Here, a new and fascinating feature appears which has no parallel in those classical situations: as we have seen, the *vector mesons* may decay to dileptons, not only after freeze-out (decoupling), but from inside the HG as well. Indeed, the dileptons emitted during the Hot Gas phase traverse the medium practically without further interaction. *Changes of the properties of these vector mesons become thus in principle observable.*

In fact, a HG is expected to affect an unstable particle in several ways: its width may increase, possibly encompassing the 'cold' mass spectrum; and its mass may shift, most likely towards lower masses in the case of the ρ. The ρ clock excess spreads now over a wider and a priori unknown mass spectrum, and may well be larger (a broader width implies an even shorter lifetime). The observed excesses could easily be reproduced by assumed medium induced changes of mass and width.

4.3 Other mechanisms may produce excesses

However, other mechanisms have also been predicted to create excesses in B-A collisions above the expectation based on p-A collisions:

i) Thermal dileptons of plausible mass distribution are expected to dominate over Drell-Yan pairs below $M \simeq 1.5$ GeV/c^2 [10].

ii) A $D\bar{D}$ enhancement in the low mass region, has been explicitly excluded, on experimental grounds [11]. But is a plausible explanation of the excess in the intermediate mass region.

iii) Secondary Drell-Yan should exist, if at all, in heavy ion collisions only, not in p-A. It considers the interaction of primary quarks of, say, the rear-guard of the projectile nuclei with secondary antiquarks just created by the vanguard [12]. The corresponding enhancement of Drell-Yan production is concentrated at low dilepton masses, due to the smaller $\sqrt{s}$ of those parton interactions.

4.4 Can experiment discriminate among mechanisms?

A limited number of tools allow us to shed some new light on some of the processes which contribute to the dimuon spectrum.

The π and K decay background can and must be studied to higher accuracy; a proven technique consists in using different absorber configurations. Mesons which decay early may give good matching fits, but when extrapolated backwards, the tracks miss the interaction point, the closest distance (offset) being large for K and small for π decays.

We have discussed the measurement of the $D\bar{D}$ component via the (small) offsets: this component exists in the $+-$ charge combination only, at SPS energies.

The various processes may be distinguishable through their slightly different p_T behaviour, at given $M_{\mu^+\mu^-}$.

The soft processes are correlated to the reaction plane of the individual event, which is measured by the Pixel spectrometer; the hard processes are not.

Finally, the ω may interfere with the ρ, allowing to shed light on their production mechanisms.

5 Detector Lifetime Under Irradiation

Let us compute the radiation load per Pb-Pb interaction. The average particle density per event, PD_{ev}, is 1/4 of the one for head-on collisions, $dN_{ch}/d\eta^{Pb-Pb}_{\text{central}} \sim 450$ [13]. With $\langle dN_{ch}/d\eta \rangle \sim 112$, and a pseudorapidity to detector surface Jacobian $d\eta/da = 1/(2\pi r^2)$, we find

$$PD_{ev} = < dN_{ch}/d\eta > \ / \ (2\pi r^2) = 18 \ / \ r^2 \tag{1}$$

The formula is derived under the (realistic) assumption of a pseudorapidity plateau throughout the phase space covered by the detectors. It yields a radiation load proportional to $1/r^2$, the inverse squared distance from the beam axis (r is in cm). The numbers take into account 14 % electrons created by photon conversion in the target of 1 mm Pb. In a much thicker target, the multiple scattering of the muons would worsen the mass resolution.

Since the useful detector surfaces extend from $r_{min} = 2.7$ mm to $r_{max} = 27$ mm, they see between 250 and 2.5 particles per event per cm^2. With 4000 pixels per cm^2, and a cluster size (number of pixels hit by one particle) of 1.3–1.4 (measured in the April '97 test), the *occupancy will vary between 8 and 0.08 %.*

With the energy loss in Si, $dE/dx = 1.7$ MeV/g/cm^2, and the dE/dx to Dose conversion factor $DCF = (dE/dx) \ / \ Dose = 6.25 \ 10^{10}$ MeV/g/krad, we find the *radiation dose* D_{10} per 10^{10} interactions:

$$D_{10} = 10^{10} \cdot PD_{ev} \cdot \frac{dE/dx}{DCF} = 5 \ krad \ / \ r^2 = 70 \ krad \cdot \left(\frac{r_{min}}{r}\right)^2 \tag{2}$$

corresponding to a maximum (at r_{min}) of 2.5×10^{12} minimum ionizing particles per cm^2.

Modern Si detectors can cope with much higher doses. In 1996, the NA50 Torino Multiplicity Detector survived, not without damage, a dose of ≈ 4 Mrad, equivalent to more than 10^{14} particles per cm^2, on the most exposed detector zones. The electronics were located a safe distance away from the beam.

In pixel detectors, the electronics chips are much more vulnerable than the detectors.

Two irradiations of LHC1 detectors took place in the NA50 beam. In November '96, two LHC1 single chip detectors were exposed to Pb-Pb interactions for 10 days; they stopped working, for unknown reasons, after receiving a dose of some 15 krad. When exposed to a β source, similar chips started losing efficiency after 15 krad.

In April '97, 4 LHC1′ chips of a modified and less vulnerable design were exposed to p-W interactions in a realistic geometry, during 3 days. After having received some 10 krad, even

the most exposed of the four had suffered no damage, in the sense that neither noisy nor dead pixels appeared during irradiation. However, since the received dose, and the induced leakage current, varied by more than a factor 10 from the corner closest to the beam to the farthest, it was not possible to find operating conditions which would preserve the efficiency of the hottest and the coolest channels at the same time.

The Microelectronics group at CERN is developing a new chip (LHC2), primarily for ALICE, based on a better transistor layout and different technology. It will incorporate an automatic compensation of the leakage current in every pixel, and allow for an individually tunable amplitude threshold. A prototype chip has been built and tested before and in the course of irradiation [7]. Its properties are not affected by doses up to 800 krad, nor by detector leakage currents corresponding to such doses. The main LHC2 detector, at 15 cm from the target and beyond (see Fig. 2, with the hottest points at $r = .45$ cm, will therefore survive at least 3 10^{11} interactions, both in terms of dose and of strongly inhomogeneous irradiation. The arrays nearer to the target, made of 2 chips each, and extending down to $r = r_{min} = .27$ cm, would receive 3 times higher doses, and must therefore be replaced several times during a run of maximal length.

Analogously, the LHC1 detector which is being assembled, will be dead after $0.8 \cdot 10^{10}$ Pb-Pb interactions, provided the first 2-chip arrays will have been replaced whenever necessary.

For p-A runs, similar limitations apply. Assuming a thermal model at a freeze–out temperature which would be the same for p and Pb beams and not depend on multiplicity, the number of produced vector mesons is proportional to $dN_{ch}/d\eta$, which determines the dose per event. The *number of good events* is then *proportional to the dose* received, *for a given detector setup*, i.e. a given acceptance. The proportionality factor is about the same for p-A and for Pb-Pb, so that statistics in p-A are a priori expensive in terms of radiation dose received. However, the p-A runs will use a setup of better acceptance than the Pb-Pb runs (see next Section); on the other hand, the aim is not to achieve similar numbers of events, but similar relative statistical errors, which means less events in p-A, since the proportion of decay background dimuons is much smaller. Finally, the results of one p-A run should match the precision of one out of several centrality bins in Pb-Pb. Under such conditions, the radiation damage from p-A runs will be much smaller than that from Pb-Pb runs.

6 Data Rate and Achievable Luminosities

While the *total number of events* is limited by the *radiation tolerance* of the detector, the main limitations to the *event rate* come from *i*) the *timing accuracy* of the Pixel spectrometer, and *ii*) by the *readout* of the vast amount of data produced.

We treat first the timing accuracy, measured by the *strobe width*, i.e. the length of the electronic signal which allows transmission of signals produced by the detector. NA50-Now has a strobe width which varies from 10 ns for the Zero Degrees Calorimeter (ZDC), to 30 ns for the Multiplicity Detector. Also, the ZDC can be used to label events which have been preceded or followed by one or more extra interactions *('pile-up')* within the Pixel detector strobe time. The LHC1 chip has a built-in option for individual timing adjustment for every pixel, resulting in a strobe width of 30 ns. Our modified 2-chip arrays used in the first plane achieve the same strobe width.

A complete system without individual pixel timing can be read with a strobe of 200 ns.

Should the LHC2 chip have a timing facility ?

The requirement of less than 20 % (signalled) events with pileup corresponds to less than 4 10^6 interactions per burst of 4 sec effective length, or 10^8 Pb ions per burst interacting with a 1.6 mm Pb target. This is a reasonable limit, compatible with the SPS Pb beam, the ZDC speed, and the requirement of optimal mass resolution. The same calculation for p-Pb runs with the event yield relative to Pb-Pb estimated at the end of the preceding Section, would yield ~ 3 events superimposed on the trigger event in the Pixel detectors; but the resulting multiplicities would still be low enough for the track matching procedure to work with good efficiency. Still, accurate timing would clearly enhance the quality of the p-A data.

To conclude, it is desirable, albeit not strictly necessary for the experimental conditions proposed here, to incorporate accurate pixel timing in the forthcoming LHC2 chip.

We come now to the readout speed. The occupancy being much higher than in NA57 or ALICE, the zero suppression facility is not used. The rate at which the pixel data are read into the VME cards is then potentially very high. The main limitation in the existing scheme comes from the fact that the data are read out and sent to the permanent storage once per event. The readout time for 2 LHC1 chips from one VME card takes 0.5 ms. Studies to speed up the readout are under way at LAPP and Saclay. It is envisaged to store several events in the existing VME cards, to derandomize the readout. It appears that the complete bit pattern can then be read and transmitted, for the full setup and for 1200 events per Pb burst, using 10 VME cards in as many crates. For the LHC2 detector, the VME cards will be equipped with burst buffers.

We consider in the following that the *data rate* limits NA50-Up to 1000 *events/burst* with LHC1 chips, and that 2 years from now, with LHC2 chips and improved readout electronics, the Pixel spectrometer can be read out at the NA50-Now rate of 4000 *events/burst.*

To translate this limit into a sensitivity, we must choose the *running conditions*, and estimate the corresponding *trigger rate.*

Fig. 14 shows the acceptance for ω dimuons versus their p_T, for various setup configurations, starting with the high mass layout used since 1995: 7 kA in the muon spectrometer's magnet, and the last 80 cm of the C hadron absorber replaced by Fe. The acceptance for low p_T ω's was 10^4 times lower than for high p_T ones. At 4 kA, a short test was done, with a 10 times higher acceptance, while the trigger rate had increased by a factor 6.5. In Section 3.2, we have shown that our simulation reproduces quite well the signal and the background spectra as well as the trigger rate (see Fig. 6). If the field in the pixel magnet is 2 T, the (dominant) low p_T muons are deflected into the NA50 acceptance, so that the acceptance for low p_T increases by another factor 10, thus becoming 1 % of the acceptance for high p_T. In this case, the trigger rate increases by only 40 %, as determined from data collected in p-W reactions in April 1997 and from simulation. For 6×10^7 Pb ions on a 1 mm Pb target, or 1.4×10^6 interactions per burst, we expect 2000 triggers/burst. These could be appropriate *running conditions for an* LHC2 *detector*, appropriate for $D\bar{D}$ physics. A 60 % running efficiency, would yield 10^{11} *interactions in a 4 weeks run*, and the results discussed in Section 3.5.

For Vector Meson physics, an even smoother p_T acceptance is preferred. For 3 kA in the muon spectrometer's magnet, 1.5 T in the pixel magnet, and 20 cm iron in the absorber, the conditions at which the main simulations presented here have been done, the acceptance varies with p_T by no more than a factor 10. The trigger rate is expected to increase in turn by an order of magnitude, so that 3×10^6 Pb ions per burst will saturate the data acquisition system; $2.5 \cdot 10^9$ *interactions in a 2 weeks run* will result, with the ρ, ω and ϕ spectra shown in Section 3.4.

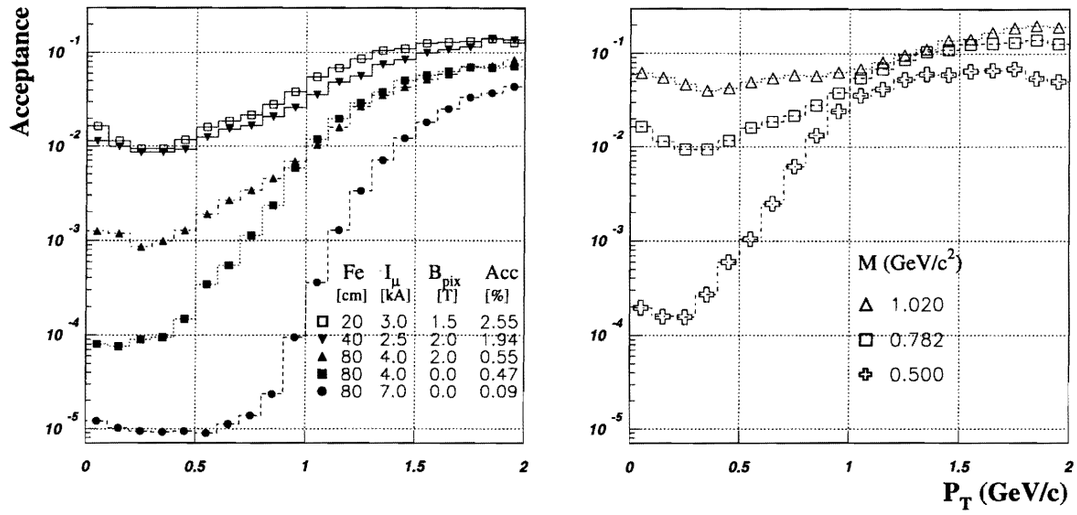

Fig. 14.: Left: Acceptance versus p_T for the ω for different field and absorber configurations. Note the gain of a factor 10 at low p_T due to the Pixel spectrometer field. The quoted total acceptance in the NA50 window corresponds to an inverse p_T slope of $T = 190$ MeV. Right: Acceptance versus p_T for 3 mass values (M_ϕ, M_ω and 0.5 GeV/c^2) in the configuration represented by open squares in the Left figure.

The configuration with 2.5 kA current in the muon spectrometer and 40 cm of Fe would give similar results. Recent simulations confirm the need for 20–40 cm of Fe at the end of the hadron absorber, for Pb–Pb collisions.

For p-A collisions, at 450 GeV/c primary beam momentum, the trigger rate is much lower, and will never saturate the data acquisition system. We will therefore take p-A data with an absorber made of carbon only, and low field in the muon spectrometer's magnet, offering high sensitivity down to low p_T.

7 Test and Data Taking Program, Beam Time Requests

A *program* has been started whose aim is the stepwise *verification* of the performance expected from the simulation, concurrently with mastery of the *technical problems* posed by the pixel technology, both general (cooling, data flow, etc.) and specific to NA50 (radiation: level and inhomogeneity).

7.1 First tests

In *November 1996*, 2 LHC1 chips (4000 pixels) were exposed during 3 weeks in NA50 to 10^7 Pb-Pb interactions per burst, for the irradiation tests described in the preceding Section.

In *April 1997*, 4 chips (8000 pixels) were set up during the RD19 tests, and then mounted in NA50 inside the refurbished and shimmed TC8 magnet, in a telescope arrangement at an angle of 75 mrad in the vertical plane, at 8, 15, 17 and 24 cm from the W target. The field map at 400 A (1.5 T) had been measured and fitted. The 60 h test allowed us to reach the main aim:

good track matching was found for $\mu^+\mu^-$ pairs, but not for Like-Sign pairs (see Fig. 15-Left).

To check that the track matching was done correctly we applied the mixed event method: the tracks in the Pixel detector were matched to muons from a randomly picked trigger. The corresponding distribution of the matching χ^2 is also shown in Fig. 15-(Left) (for the same statistics).

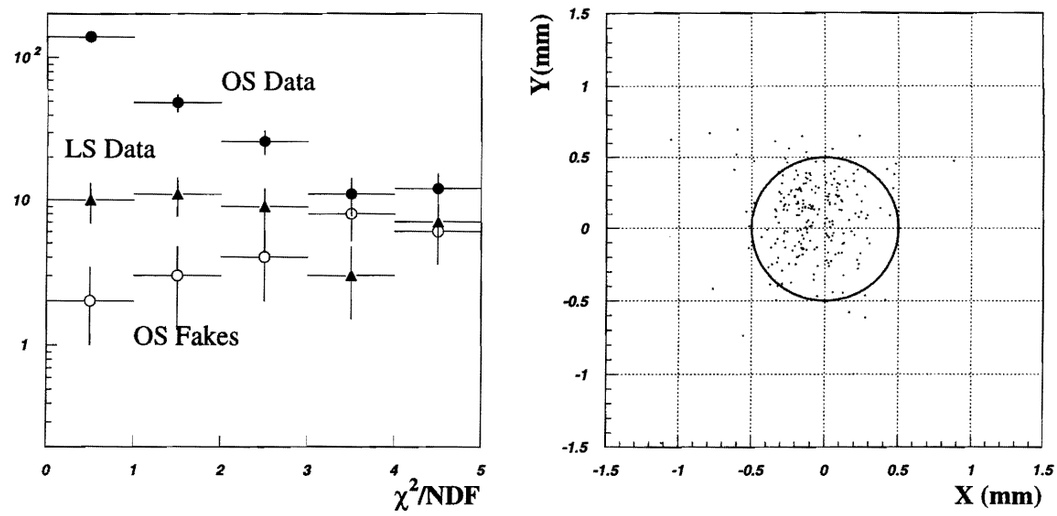

Fig. 15.: Results of the April 1997 track matching test: (Left) χ^2 distributions for matched NA50 muons from Opposite-Sign (OS) and Like-Sign (LS) pairs. The solid symbols represent the original data. The open circles are normalized fakes contributions to OS, obtained by matching NA50 muons to pixel tracks from different events. The difference between the top and the sum of the lower distributions represents the genuine muon matches. (Right) Extrapolation of matched tracks (OS sample) in the X-Y plane to the centre of the target. The circle corresponds to the 1 mm diameter target. The distribution corresponds to expectation.

Fig. 15-Right shows the extrapolation of the matched tracks to the centre of the 1 cm long W target in the X–Y plane. The outline of the 1 mm diameter target is also shown. The horizontal standard deviation is due to the pixel size of 500 μm, while the vertical one results from the target length.

Also, a simple pixel safety system suggested by L. Gatignon was set up and found to work satisfactorily. When in one instance the beam became suddenly unstable, the halo counter exceeded the maximal allowed counting rate, which caused a beam magnet to stop, so that starting from the following burst, no beam reached the NA50 zone. An even faster safety system is being studied.

7.2 Present and future plans

A new high precision support allows the Pixel spectrometer to be installed and to be removed in a couple of hours, so that NA50-Up tests can alternate with NA50 physics runs.

For the *fall of 1997*, we plan to install *4 half-planes* (34 chips, 70 kpixels), in order to measure *muon pairs*. In 5 days of proton beam it should be possible to set up and test the detector and to measure the *mass resolution* and the *background rejection*.

Table 1: Beam time requests (1st figure for setting up, 2nd for data taking), radiation load, and expected numbers of Signal events S. Errors are statistical, $\sigma(S) = \sqrt{S+B}$ for resonant and $\sigma(S) = \sqrt{S+2\cdot B}$ for nonresonant signal. The background events B are due to π and K decays, plus, for ω events, some ρ's and the continuum. The dose refers to the hottest region of station 2 (the few detectors of station 1 may be replaced during a run). Layout: the absorber is all carbon for p beam; with Pb beam there is 20 [80] cm Fe with LHC1 [LHC2] detector. I(ACM magnet)=4 kA for the LHC2 Pb-Pb run, 3 kA otherwise.

Beam, target per burst [mm]	Time [days]	Dose [krad]	ω $(.75 < M < .82)$: $S \pm \sigma_S$, B/S $p_T < .6$ GeV/c	$p_T > .6$ GeV/c	$D\bar{D}$ $(1.2 < M < 2.5)$ $S \pm \sigma_S$, B/S
1997, April: 8192 LHC1 channels; October: 69 632 channels					
10^8 p, 10 W	*done*	4	April Test: track matching, radiation tolerance		
$5\cdot 10^7$ p, 20 Be	3/2	1.5	November Test: dimuon mass resolution, 1000 ω's		
1998 : 131 072 LHC1 channels, 2.5 $\cdot 10^9$ Pb-Pb interactions, for vector mesons					
10^8 p, 20 Be	4/2	2.5	2000 ± 60, .13	4500 ± 75, .12	-
$4\cdot 10^8$ p, 1 Pb	2/2	2.5	1600 ± 55, .20	3600 ± 70, .16	-
$6\cdot 10^6$ Pb, 1 Pb	2/12	7	1700 ± 100, 4.5	6500 ± 140, 2	-
1999–2000 : LHC2 detector, 10^{11} Pb–Pb interactions, for $D\bar{D}$ and high p_T					
10^9 p, 20 Be	4/2	25	$20\,000 \pm 160$, .13	$45\,000 \pm 240$, .12	200 ± 28, 1.3
$4\cdot 10^9$ p, 1 Pb	2/2	25	$16\,000 \pm 150$, .20	$36\,000 \pm 220$, .16	500 ± 32, 0.6
$6\cdot 10^7$ Pb, 1 Pb	2/26	300	5000 ± 150, 3.5	$60\,000 \pm 400$, 1.6	2500 ± 220, 20

We intend to complete and test the 64 chip LHC1 Pixel detector (Fig. 2) by April 1998, and to take *Vector mesons physics* data during the 1998 Heavy Ion run, at a reduced luminosity, but with good acceptance down to $p_T = 0$ (top curve on Fig. 14). We expect to have a first glance at the lifetime of the hot hadron gas phase, and to approach the question of whether mass and width of hadrons are given once for ever, or depend on the medium.

The detector will be destroyed by the same particles which it is set up to measure. When the LHC2 chips and the corresponding readout electronics will be available, in principle already in 1999, they should replace the LHC1 detectors. A setup fully equipped with LHC2 chips, capable of track extrapolation back to the vertex (see Fig. 2), and not limited any more by radiation damage, should yield much improved statistics, in particular at high mass and high p_T. Also, the measurement of Open Charm production becomes possible.

7.3 p-A programme

If successful, the proposed upgrade will have unprecedented mass resolution, $D\bar{D}$ identification, and statistical accuracy. A complete program includes therefore necessarily a handsome p-A program, whose main aims are:

i) measuring the $\rho - \omega$ interference phase, its p_T dependence, and its possible A dependence;

ii) the $D\bar{D}$ production cross section and its A dependence.

We envisage a first exploratory program of 3-4 weeks, spread over two years, to measure dimuon production in p-Be and p-Pb collisions at 450 GeV/c. The possibility of measuring p-p and p-d reactions is being studied.

7.4 Beam time requests

The beam time requests *specific to the Pixel Spectrometer Upgrade* are detailed in Table 1, and listed hereafter for 1997–1998:

i) 5 days of p beam in November 1997, to check the mass resolution of a halfsized detector

ii) 10 days of p beam in 1998, for setting up the full detector, and for p-A reference data

iii) 14 days of Pb beam in 1998, to evaluate the spectrometer, and take vector meson data.

With a detector equipped with LHC2 chips, we will require, not before 1999,

iv) a short period with p beam, months before the Pb beam, for LHC2 detector tests;

v) 10 days of proton beam, for high luminosity p-A reference data, and

vi) several weeks of Pb beam, for high luminosity, dominantly high p_T dimuon physics.

8 Responsibilities and Budget

The budget has so far been kept rather low, thanks to recycling of existing equipment (magnet, cooling system, cables) and use of detectors built and tested for WA97 and NA57, but rejected because of one or more chips malfunctioning among the 6 of a ladder. This was possible since we use exclusively incomplete ladders, plus a few single chip detectors (see Fig. 2).

The budget needed to build the vertex spectrometer based on LHC1 chips amounts now to 100 kCHF, to be spent in 1998. The responsibilities are shared among the groups from CERN and Lisbon (simulation, detectors, magnet, protection, detector monitoring), Yerevan (detector supports and ladder cutting), Lyon (mechanical structure), Annecy and Saclay (readout), Lisbon and Annecy for data acquisition, and Troitsk (temperature controls and safety).

Manpower is not included.

The budget for the LHC2 version will include the cost of the detectors and of a fast VME readout to be developed by Saclay and Annecy. Its amount will be of the order of 250 kCHF, to be spent in principle mainly in 1999.

Acknowledgements

The rapid progress of the program outlined above has been possible thanks to the farsightedness of E. Heijne and P. Jarron and their group, who created the Pixel detector, and to the

timely development, for and by RD19 and the WA97/NA57 experiments (E. Quercigh and F. Antinori), of chip assemblies of properties and dimensions rather exactly matched to our needs.

W. Flegel found and overhauled an appropriate magnet, whose field was measured by F. Bergsma, P. Akishin (Dubna) having computed the shims. We got assistance from J.P. Avondo, A. Beer, C. Millerin, R. de Oliveira, for cables, detectors and electronics, Y. Lesénéchal who provided the cooling system, Harry Beker and Alessandra Mazzoni for Data Acquisition, and many others. J. Schukraft has encouraged us from the start, and U. Heinz has been a precious theory adviser. We thank them all.

This work is partially supported by INTAS grant N° 96-0231.

References

1. U. Heinz, K.S. Lee, Phys. Lett. **B 259** (1991) 162; Nucl. Phys. **A544** (1992) 503c.
2. A.A. Grigorian, P. Sonderegger, *"Physics of low mass dileptons produced in heavy ion collisions"*, Technical Note NA50-Up 97/1.
3. A. Drees, Nucl. Phys. **A610** (1996) 536c.
4. M.C. Abreu *et al.*, Phys. Lett. **B368** (1996) 230.
5. M.C. Abreu *et al.*, accepted by Phys. Lett. B.
6. E. Heijne *et al.*, CERN-ECP/96-03, 5 Jan 1996.
7. W. Snoeys, forthcoming RD19 Status Report.
8. C. Lechanoine, M. Martin, H. Wind, NIM **69** (1969) 122.
9. See QM96 proceedings, Nucl. Phys. **A610** (1996). In particular: U. Heinz, p. 264c; A. Franz *et al.*, p. 240c; K. Kadija *et al.*, p. 248c; L. Rosselet *et al.*, p. 256c.
10. P.V. Ruuskanen, Nucl. Phys. **A525** (1991) 255c.
11. P. Braun-Munzinger *et al.*, nucl-ex/9704011 (CERN-PPE/97-65), accepted by Z. Phys. C.
12. C. Spieles et al., hep-ph/9706525 (LBNL-40497), submitted to Z. Phys. C.
13. P.G. Jones *et al.*, Nucl. Phys. **A610** (1996) 188c.